ELSEVIER

Journal of Alloys and Compounds 320 (2001) 151–160

Journal of ALLOYS AND COMPOUNDS

www.elsevier.com/locate/jallcom

Calculated phase diagrams of aluminum alloys from binary Al–Cu to multicomponent commercial alloys

X.-Y. Yan[a,*], Y.A. Chang[a], F.-Y. Xie[a], S.-L. Chen[b], F. Zhang[b], S. Daniel[b]

[a]*Department of Materials Science and Engineering, University of Wisconsin, 1509 University Ave., Madison, WI 53706, USA*
[b]*CompuTherm, LLC, 437 S. Yellowstone Dr., Suite 217, Madison, WI 53719, USA*

Abstract

More than three decades have passed since the publication of Alan Prince's book on multicomponent phase equilibria. The most significant development in this time has been the use of a combined computational/experimental approach to calculate multicomponent phase diagrams. This has led to important advances in the design and processing of structural and functional materials for practical applications. In this paper, we present a few examples focusing on aluminum alloys from the classical Al–Cu binary to multicomponent alloys with a view toward practical applications.

Keywords: Multicomponent phase diagrams; Computational/experimental approach; Al–Cu binary

1. Introduction

Since the classical book by Alan Prince on *Alloy Phase Equilibria* [6], advances in this field have been made primarily in the use of a combined computational/experimental approach to obtain multicomponent alloy phase diagrams. In this approach, thermodynamic descriptions of constituent binaries of a multicomponent system are developed first relying primarily on experimentally determined thermodynamic and phase equilibrium data. The term thermodynamic description of a system means that a set of thermodynamic model parameters for all phases involved is obtained such that not only the phase diagram but also the single phase thermodynamic properties can be calculated (e.g. Ref. [7]). The parameters should be obtained from extensive and reliable experimental data. However, in many alloy systems extensive experimental data are not available and judgement needs to be made in constraining these parameters either by experience or semi-empirical correlations (e.g. Refs. [8,11]) or both. On the basis of the binary descriptions and ternary experimental data, thermodynamic descriptions of ternaries can be readily developed in a manner similar to that for binaries using one of the geometrical models (e.g. Ref. [16]) to extrapolate the Gibbs energies of binary to ternary solution phases. Moreover, when reliable binary descriptions are developed, ternary parameters introduced are normally small. This implies that interactions for quaternary and higher order systems are anticipated to be even smaller and may be ignored. If quaternary and higher order phases do not exist, this approach allows us to compute phase diagrams of higher order systems based only on the descriptions of constituent binaries and ternaries. In essence this approach becomes a powerful tool in obtaining phase diagrams of multicomponent systems for technological applications.

It is well known that quaternary phases rarely exist in practice with relatively few exceptions [3]. However, when they do exist in systems of interest, the experimental data must be used to develop descriptions of these quaternary systems. But the effort involved usually turns out to be much less challenging than that for binary and ternary systems. Nevertheless, multicomponent phase diagrams obtained in this manner must be verified experimentally. But the effort involved is greatly reduced when compared to purely relying on experimental investigations as has been done in the past. The calculated phase diagrams serve as an intelligent guide to focus on a few alloys for experimental investigation. For example, Liang [23] had recently carried out experiments to measure the solid/liquid phase boundaries of quaternary Al–Cu–Mg–Zn alloys experimentally in the aluminum rich corner. It was found that the experimentally determined values are indeed in accord with those calculated, at least for this quaternary system.

After the thermodynamic description for an alloy system

*Corresponding author.

0925-8388/01/$ – see front matter
PII: S0925-8388(00)01469-9

is developed, thermodynamic calculation software is used to calculate the phase diagrams and thermodynamic properties. Although the basic principles for calculating phase diagrams have been known for more than a half-century, only recent advances in computational methods and the availability of fast computers have made the calculations possible. The calculated phase diagrams provide a road map for materials and processing development such as in metal casting and subsequently thermal mechanical treatments in order to produce materials with the appropriate microstructures and mechanical properties.

In the present study, we will present several examples of the rapid advances being made in obtaining phase diagrams using the combined computational/experimental approach with a view toward utility either for research in an allied field or for practical applications in alloy and processing developments. We will focus primarily on aluminum alloys, but the approach is equally valid for other alloys. The examples presented begin with the classical binary Al–Cu to multicomponent Al–Cu–Fe–Si–Mg–Mn–Zn alloys. We will present in Section 2.1, the importance of reliable binary descriptions for obtaining descriptions of higher order systems; in Section 2.2, a comparison of calculated phase diagrams of quaternary Al–Cu–Mg–Si with experimental data; in Section 2.3, a calculated isopleth of Al–Mg for the quinary Al–Mg–Fe–Mn–Si system as well as a comparison of the calculated solidification path of alloy 5182, Al–4.74%Mg–0.1%Si–0.28%Fe–0.34%Mn, with experimental data; in Section 2.4, a calculated isopleth of Al–Cu for the six-component Al–Cu–Fe–Mg–Si–Zn system and the heat of evolution during the course of solidification of alloy 7075, Al–1.36%Cu–0.28%Fe–2.49%Mg–0.11%Si–5.72%Zn; and lastly in Section 2.5, a calculated isopleth of Al–Cu for the seven-component Al–Cu–Fe–Mg–Mn–Si–Zn system and the phase fractions as a function of temperature for alloy 390, Al–15%Si–5.5%Cu–0.65%Mg–0.3%Fe–0.01%Mn–0.065%Zn. In the present paper, all compositions are given in wt.% unless noted otherwise. All calculations for phase diagrams, paths of solidification, heats of evolution as well as the phase fractions are carried out with PANDAT [28].

2. Examples

2.1. Importance of binary descriptions

Recently Xie et al. [24] studied the degrees of microsegregation in Al-rich Al–Cu–Mg alloys experimentally using directional solidification and computationally using a modified Scheil model which incorporates coarsening of the dendrites, back diffusion in the solid, and the effect of undercooling. They found discrepancies existed between the model-calculated concentration distributions of Cu in the dendrite arms and the results obtained from directional solidification. The phase diagram data required to carry out the calculation were obtained from the ternary thermodynamic description by Chen et al. [22]. An examination of the calculated solidus curve of (Al) shown as a dashed line in Fig. 1 showed that the calculated solubility of Cu along the isopleth of Al–$Cu_{0.5}Mg_{0.5}$ was as much as 0.5 mol.% lower than the experimental data [15]. Xie et al. attributed the discrepancies, between the calculated and experimentally determined concentration distributions in the dendrite arms, to the inaccurate solidus surface of (Al) calculated from the description of Chen et al. [22]. The inadequacy of the ternary description was a result of using the binary Al–Cu description from the literature [18,20].

Subsequently, Liang et al. [25] showed that this was indeed the case and provided an improved description first for the Al–Cu binary and then that for the Al–Cu–Mg ternary. As shown in Fig. 2, the calculated solidus curve of (Al) in the Al–Cu binary using the description of Liang et al. is in accord with the five sets of data [1,25,30–33], except for the data of Matsuyama [1] which is in error [12]. Yan et al. [26] recently studied the degree of microsegregation in an Al–4.5Cu alloy using directional solidification. Comparisons of the calculated concentration profiles of Cu in the dendrite arms as fractions of solids using the modified Scheil model [24] and the thermodynamic descriptions of Saunders [18,20] and Liang et al. [25], respectively, are given in Fig. 3 with the experimental data [26]. It is evident from this figure that calculated results using the improved description is in better agreement with the experimental data. The discrepancies in the solubility of Cu in (Al) are less than 0.25 mol.%. A similar

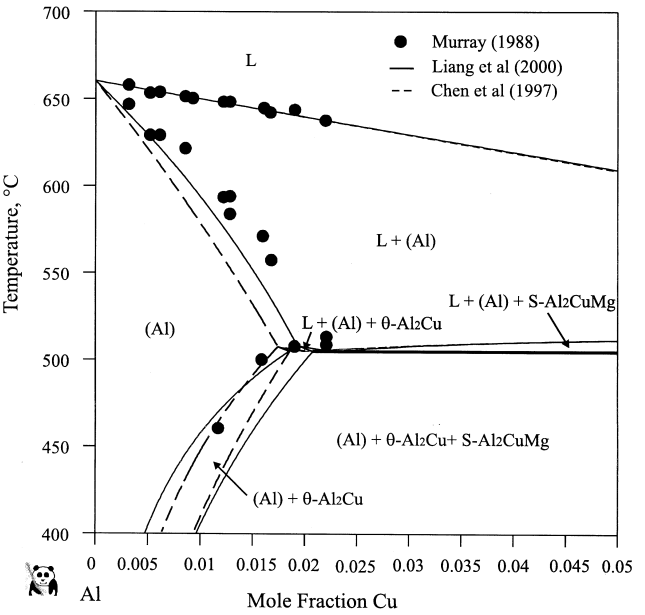

Fig. 1. Comparison of the experimental liquidus and solidus along the isopleth Al–$Cu_{0.5}Mg_{0.5}$ with those calculated using the description of Chen et al. [22] shown as dashed lines and those of Liang et al. [25] shown as solid lines.

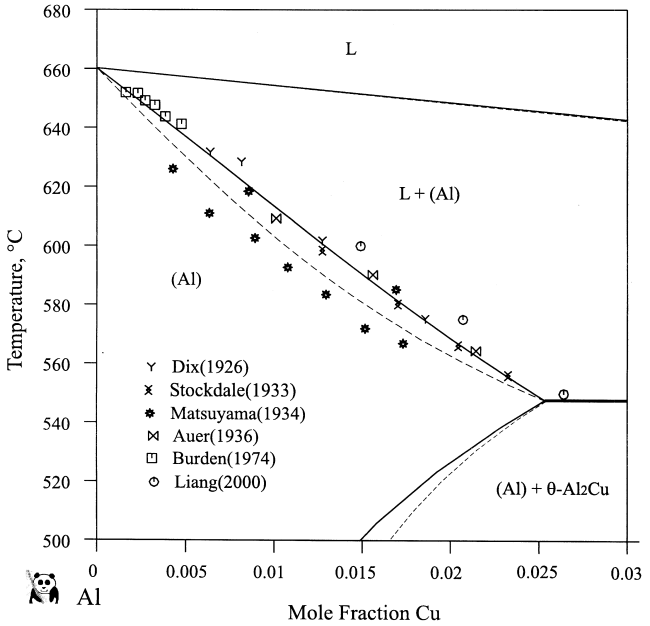

Fig. 2. Comparison of the experimental solidus data for the (Al)+liquid equilibrium in binary Al–Cu with the calculated solidus. The dashed lines are calculated using the description of Saunders [18,20] while the solid lines using the improved description of Liang et al. [25].

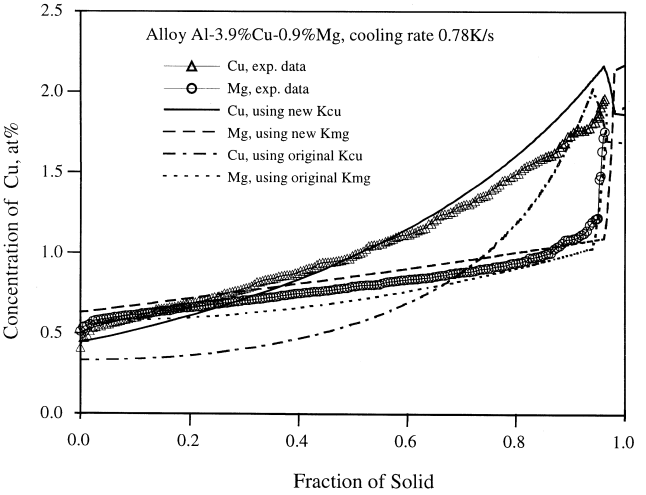

Fig. 4. Comparison of the experimental concentration profiles of Cu and Mg in a directionally solidified Al–3.9Cu–0.9Mg alloy at a cooling rate of 0.78 K/s [24] with the model-calculated values using the phase diagram data or K (the partition coefficients) obtained from the description of Chen et al. [22] (denoted as using original K) and those using the partition coefficients obtained from the improved description of Liang et al. [25] (denoted as using new K).

comparison for the ternary Al–3.9Cu–0.9Mg alloy is presented in Fig. 4 and the same conclusion can be reached. These results demonstrate that (i) a good thermodynamic description of a constituent binary is necessary to obtain a good description of a ternary system and (ii) accurate phase diagram data are needed in order to test the validity of a kinetic model in studying microsegregation in alloys.

2.2. Quaternary Al–Cu–Mg–Si system

Since the basic elements in the 2000 series of aluminum alloys are Al, Cu, Mg, and Si, we present in this section one calculated isopleth and one isotherm of this quaternary

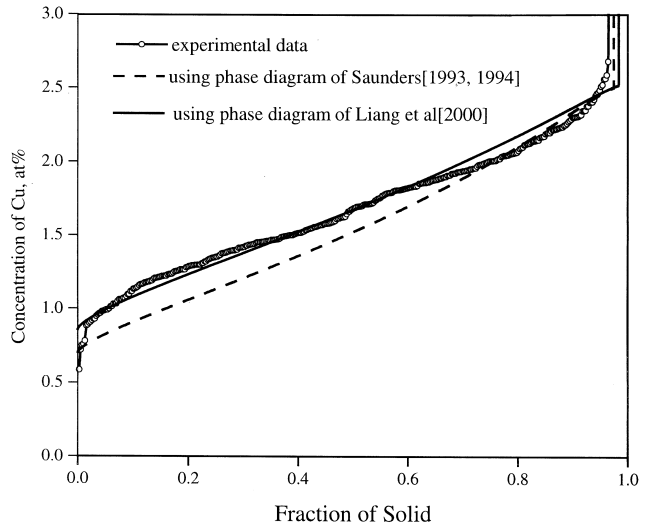

Fig. 3. Comparison of calculated Cu concentration profiles in the dendrite arms using two sets of phase diagram data with experimental results for an Al–4.5Cu alloy directionally solidified at a growth rate of 0.05 mm/s and a temperature gradient of 50 K/cm.

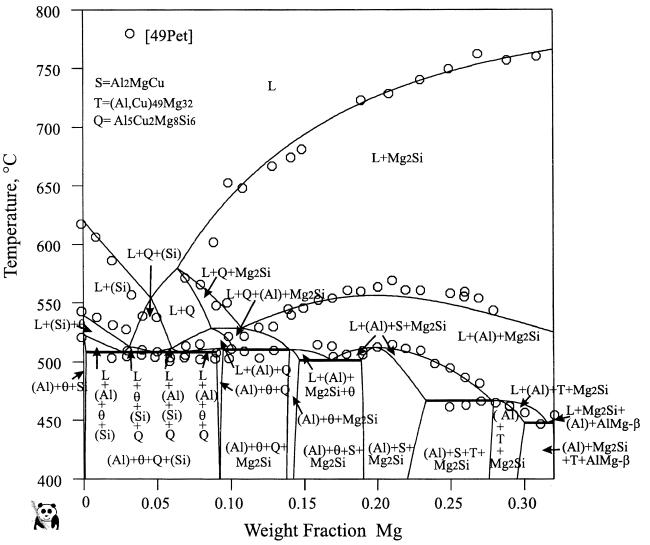

Fig. 5. Comparison of a calculated isopleth of Cu–Mg for Al–Cu–Mg–Si with fixed values of 60% Al and 8% Si with the experimental data of Petrov et al. [2].

using a thermodynamic description developed by Yan [27]. Since a quaternary phase $Al_5Cu_2Mg_8Si_6$ exists, it was necessary to also model the quaternary system in addition to modeling the constituent ternaries and binaries. However, the effort involved in modeling this quaternary is minimum. Fig. 5 shows a comparison between the calculated isopleth of Cu–Mg with fixed values of 60% Al and 8% Si and the data obtained experimentally [2]. Good agreement is achieved. Table 1 shows a comparison of several calculated invariant equilibrium temperatures with experimental data. Good agreement is again attained. As shown in Fig. 6, the calculated 500°C isotherm is also in accord with experimental data [4].

2.3. Quinary Al–Mg–Fe–Mn–Si system

The alloy AA5182 is an aluminum alloy containing Mg, Fe, Mn and Si as the alloying elements. It is a strain-hardening alloy with Mg contents varying from 4 to 5%. Fig. 7A shows a calculated isopleth of Al–Mg from pure Al to 70 mol.% Mg with fixed values of 0.28% Fe, 0.34% Mn and 0.1% Si. This isopleth is calculated using PANDAT [28] without providing any initial values. It is only necessary to specify (i) the intended compositions of Fe, Mn and Si fixed at 0.28%, 0.34% and 0.1% respectively, (ii) the intended temperature range from 400 to 1000°C, and (iii) the intended compositional range of Mg, from 0 to 70 mol.%. The isopleth shown in Fig. 7A is then automatically calculated using a multicomponent aluminum database [29]. It is interesting to note that the topology of the phase equilibria in the mid composition range as shown in Fig. 7A is quite similar to that in binary Al–Mg as shown in Fig. 7C [19].

The composition of the alloy AA5182 investigated by Backerud et al. [17] is indicated as a dashed line in Fig. 7A and B. The latter figure is an enlarged portion of the isopleth shown in Fig. 7A with the Mg content varying

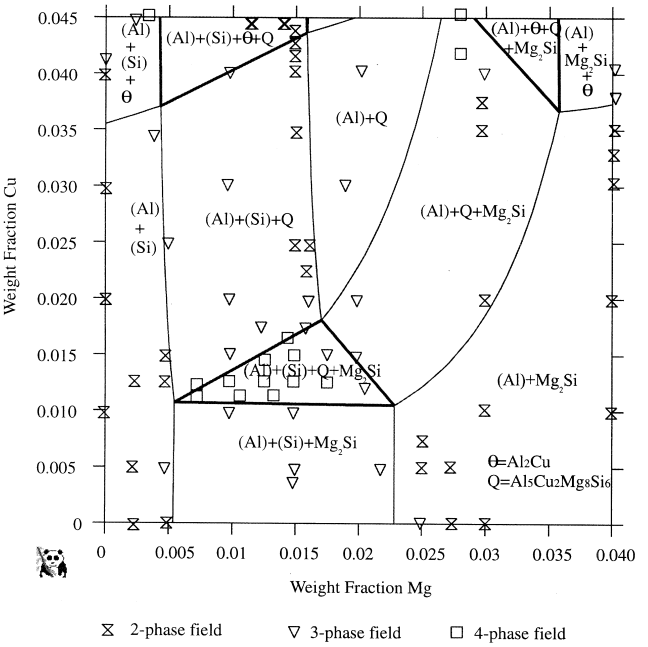

Fig. 6. Comparison of a calculated 500°C isotherm of Al–Cu–Mg–Si with a fixed value of Si-1.8% with experimental data obtained from Smith [4].

from 0 to 10 mol.%. As shown in Fig. 7B, the sequence of phases formed when this alloy solidifies under equilibrium condition is: $L \rightarrow L+Al \rightarrow L+Al+Al_{13}Fe_4 \rightarrow L+Al+Al_{13}Fe_4+Mg_2Si \rightarrow Al+Al_{13}Fe_4+Mg_2Si \rightarrow Al+Al_{13}Fe_4+Mg_2Si+Al_6Mn$. Solidification begins at 634°C and ends at 576°C with a freezing range of 58°C. The freezing range under actual cooling conditions would be larger due to microsegregation. A comparison of the calculated temperatures for the various reactions under equilibrium and Scheil conditions are summarized in Table 2 with the experimental data of Backerud et al. [17]. Reasonable agreement is obtained between the calculated and experimental results.

Table 1
Comparison of calculated invariant equilibrium temperatures (°C) with experimental data in the Al–Cu–Mg–Si system

Equilibrium	Experimental	Calculation
$L+Mg_2Si=(Al)+(Si)+Al_5Cu_2Mg_8Si_6$	521 [2] 529 [10]	524
$L+Mg_2Si=(Al)+\theta\text{-}Al_2Cu+Al_5Cu_2Mg_8Si_6$	510 [14] 513 [21]	511
$L=(Al)+\theta\text{-}Al_2Cu+(Si)+Al_5Cu_2Mg_8Si_6$	510 [2] 512 [5] 505 [2] 506.5 [14] 507 [5] 510 [21]	509
$L=(Al)+\theta\text{-}Al_2Cu+Mg_2Si+S\text{-}CuMgAl_2$	500 [2] 507 [5] 500 [14]	502
$L+S=(Al)+Mg_2Si+T\text{-}CuMg_4Al_6$	464 [2] 467 [10]	467
$L=(Al)+\beta\text{-}Mg_5Al_8+Mg_2Si+T\text{-}CuMg_4Al_6$	444 [2] 444–448 [10]	448

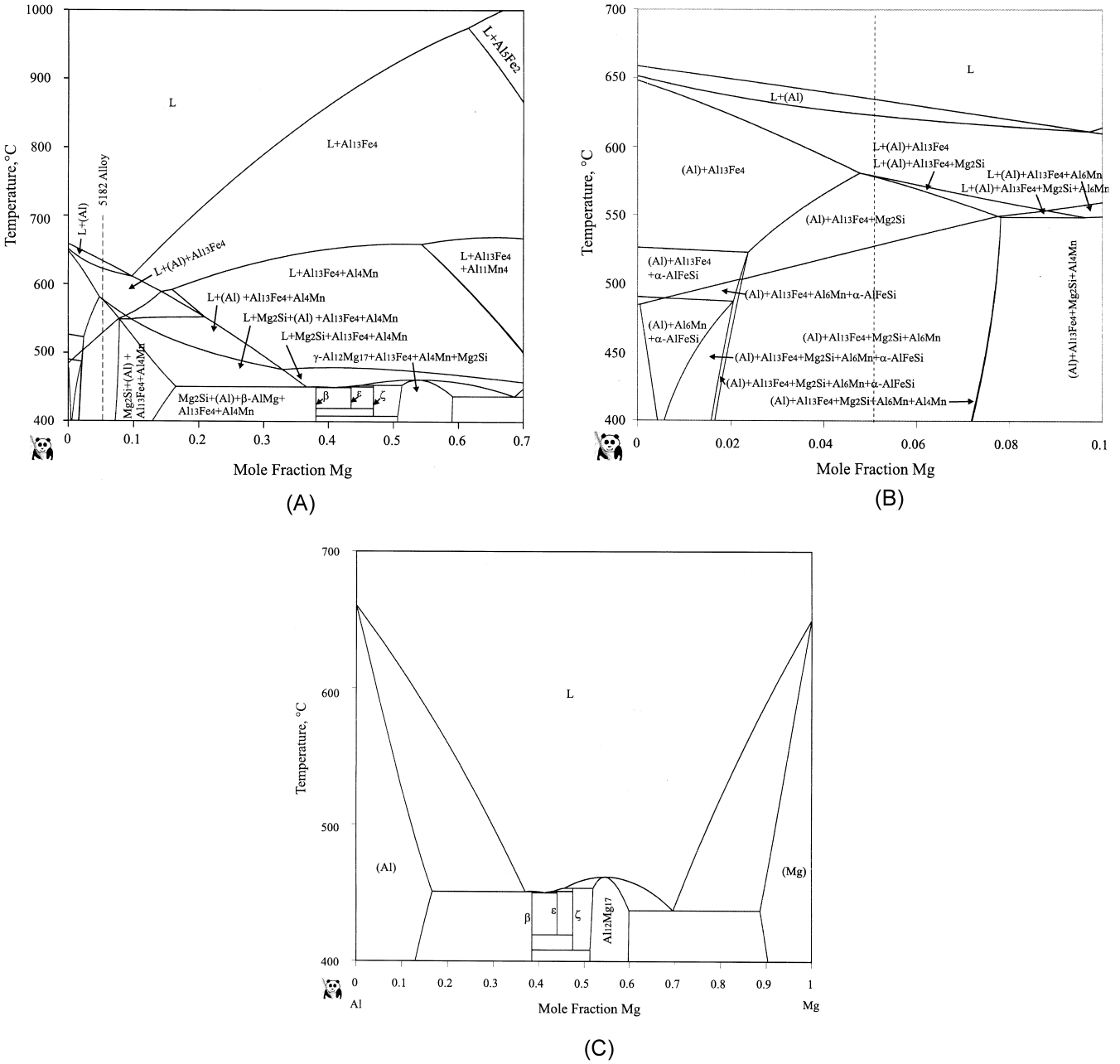

Fig. 7. (A) A calculated isopleth of Al–Mg with fixed values of 0.28% Fe, 0.34% Mn and 0.1% Si. (B) A calculated isopleth of Al–Mg with fixed values of 0.28% Fe, 0.34% Mn and 0.1% Si in the Al-rich portion of the isopleth shown in (A). (C) A calculated binary Al–Mg phase diagram [19].

Table 2
Comparison of calculated solidification temperatures under global equilibrium and Scheil condition with experimental value of Ref. [17] for A5182 alloy

	Experiments with cooling rates between 0.3 and 11°C/s [17]	Equilibrium condition	Scheil condition
First reaction *T*, °C	632–623	634	634
Second reaction *T*, °C	621–617	622	622
Third reaction *T*, °C	586–571	578	556
Fourth reaction *T*, °C	557–470[a]		451
End of solidification, °C	470[a]	576	451
Solidification range, °C	162	58	183

[a] Estimated value from the Al–Fe–Si phase diagram.

We will in a later section present a comparison of the calculated freezing temperature ranges under equilibrium and Scheil conditions with experimentally determined values for this quinary alloy as well as for two higher order aluminum alloys followed by a brief discussion.

2.4. Six-component Al–Cu–Mg–Si–Fe–Zn system

Fig. 8A shows a calculated isopleth of Al–Cu for this six-component Al–Cu–Mg–Si–Fe–Zn system from 0 to 60 mol.% Cu with fixed values of 2.47% Mg, 0.11% Si, 0.28% Fe, and 5.72% Zn using the same database as the AA5182 alloy [29]. In view of the complexity of the phase relationships, phase fields are not labeled in this figure but the information can be readily obtained from PANDAT [28]. The Al-rich portion of the phase diagram given in Fig. 8A is enlarged for clarity and shown in Fig. 8B from 0 to 5 mol.% Cu with the phase fields labeled. As shown in Fig. 8B, it is difficult to resolve all the phase equilibrium features at temperatures above and below 480°C. Accord-

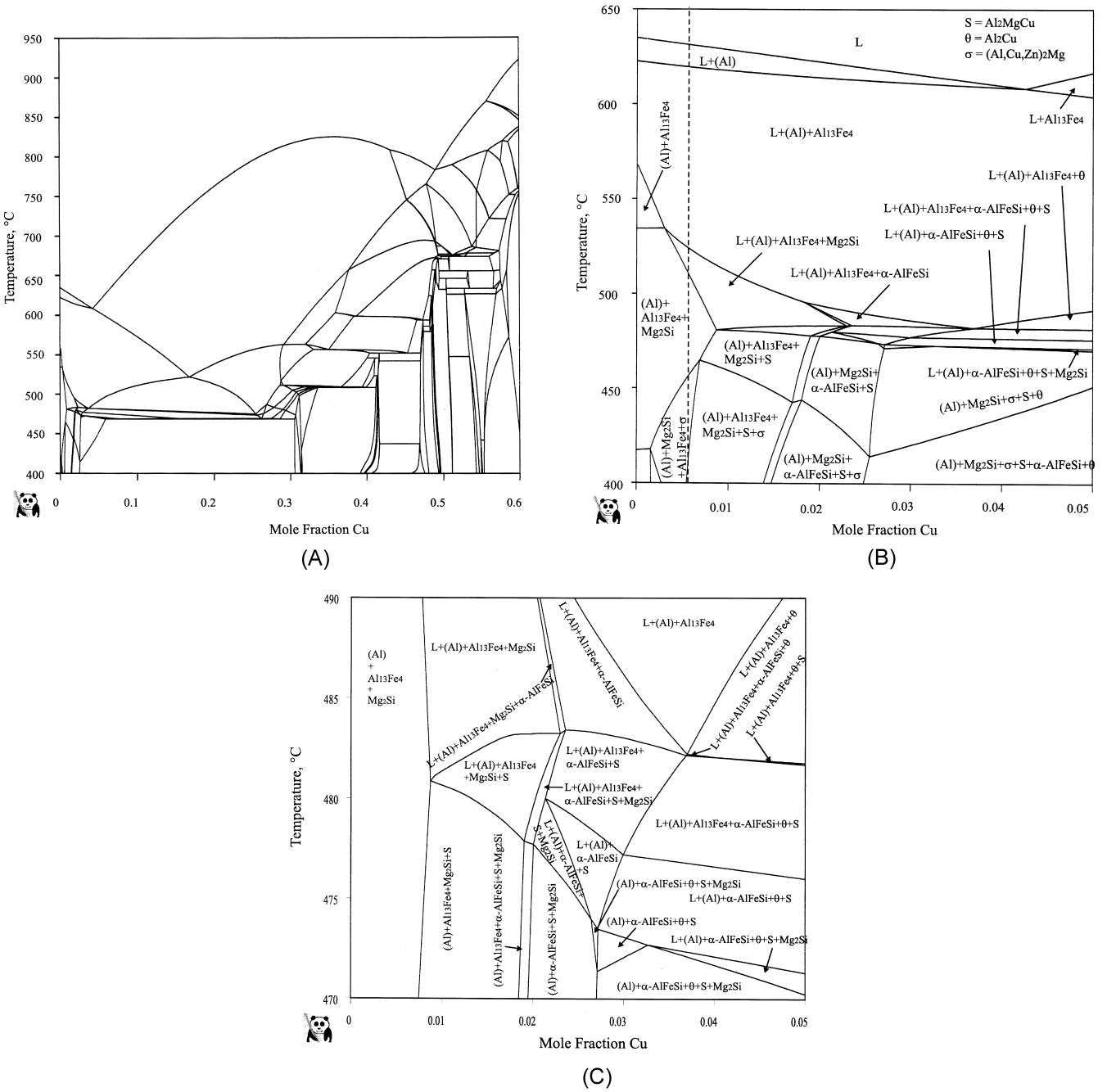

Fig. 8. (A) A calculated isopleth of Al–Cu with fixed values of 0.28% Fe, 2.49% Mg, 0.11% Si and 5.72% Zn. (B) Al-rich portion of the isopleth given in (A). (C) Enlargement of (B) in the temperature interval between 470 and 490°C.

ingly, phase equilibria in that region are further enlarged and shown in Fig. 8C. The enlarged diagrams in Fig. 8B and C should facilitate readers. The composition of the alloy 7075 is shown as a dashed line in Fig. 8B being Al–1.36%Cu–0.28%Fe–2.49%Mg–0.11%Si–5.72%Zn. Calculation of the Al–Cu isopleth for this six-component system is similar to that for the quinary system except it is necessary to fix the composition of four components.

Fig. 9 shows a comparison of the calculated temperatures as a function of the fraction of solids formed using the Scheil model with experimental data obtained from thermal analysis [13]. Good agreement is obtained between the calculated results and experimental data for the six-component alloy 7075. In addition, the heat evolution during the course of solidification under the Scheil condition is presented in Fig. 10 as a function of temperature from 631 to 473°C, at which the alloy is completely solidified. The amount of heat evolved as shown in this figure is considerably more exothermic than the heat of freezing of pure aluminum, −10.8 kJ/mol [9].

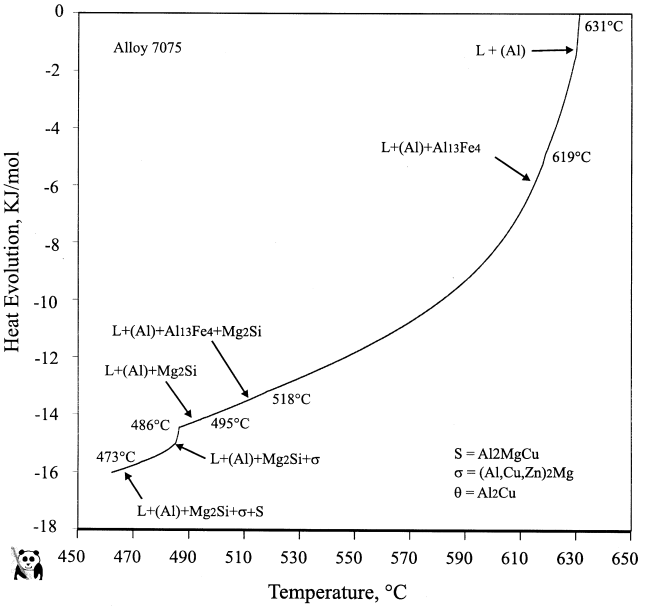

Fig. 10. Calculated heat of evolution of the alloy 7075 as a function temperature as a result of phase transformation during the course of solidification under the Scheil condition.

2.5. Seven-component Al–Cu–Mg–Si–Fe–Mn–Zn system

In a similar manner as for the quinary system in Section 2.3, an isopleth of Al–Cu for the seven-component Al–Cu–Mg–Si–Fe–Mn–Zn system is calculated using PANDAT with the exception that we have to fix the compositions of five components. The calculated isopleth is shown in Fig. 11A as a function of the composition of Cu from 0 to 65 mol.% Cu, with fixed compositions of 0.3% Fe, 0.65% Mg, 0.01% Mn, 15% Si, and 0.065% Zn. As is done for Fig. 8A, phase fields are not labeled in view of the complexity of the phase equilibria. Since commercial aluminum alloys consist of primarily the (Al) solid solution phase with other phases present in minority quantities, an enlarged portion of the Al-rich phase equilibria in Fig. 11A is redrawn and shown in Fig. 11B, displaying only the phase equilibria from 0 to 20 mol.% Cu. The composition of the alloy A390 being Al–15%Si–5.5%Cu–0.65%Mg–0.3%Fe–0.01%Mn–0.065%Zn is shown in Fig. 11B as a dashed line.

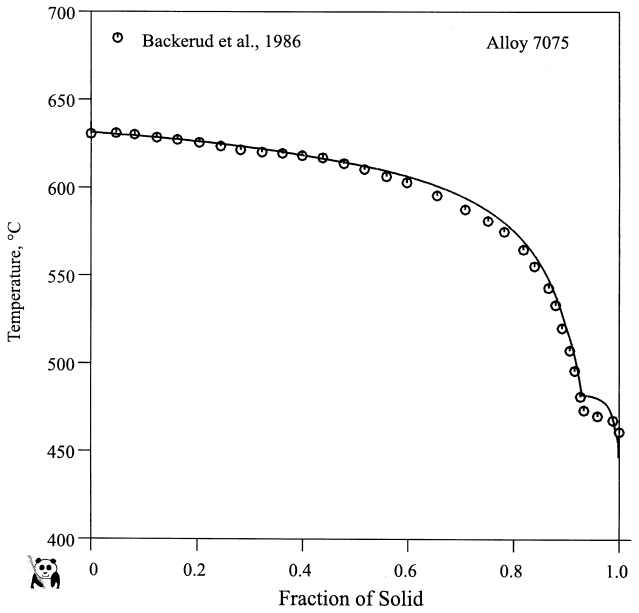

Fig. 9. Comparison of the calculated fractions of solid as a function of temperature of the alloy 7075 with the experimental data from Backerud et al. [17].

Let us first examine the phase fields in this diagram focusing on the region marked ‘B’ prior to carrying out solidification-type calculations for alloy 390. Immediately to the left of ‘B’ there is a three-phase field of L+(Si)+β-AlFeSi and to the bottom of ‘B’, a four-phase field of L+(Si)+β-AlFeSi+θ. This is consistent with the rule of isopleth construction since the number of phases increases by one when crossing from one phase field to a neighboring one. In this case, the number of phases increases by 1 from 3 to 4. On the other hand, just above ‘B’ there is a three-phase field of L+(Si)+δ-AlFeSi and to the left of ‘B’ as noted above there is another three-phase field of L+(Si)+β-AlFeSi. This is inconsistent with the rule of isopleth construction; two three-phase fields cannot be adjacent to each other. How can we reconcile this discrepancy or apparent discrepancy as shown in this figure? Is there an error made by PANDAT? Is the basic calculation engine of PANDAT unreliable? However, when we zoom onto the region ‘B’, the apparent discrepancy disappears! Graphical representation of the phase equilibria in the space marked ‘B’ is enlarged and shown in Fig. 11C. We note in this figure that indeed there is a four-phase

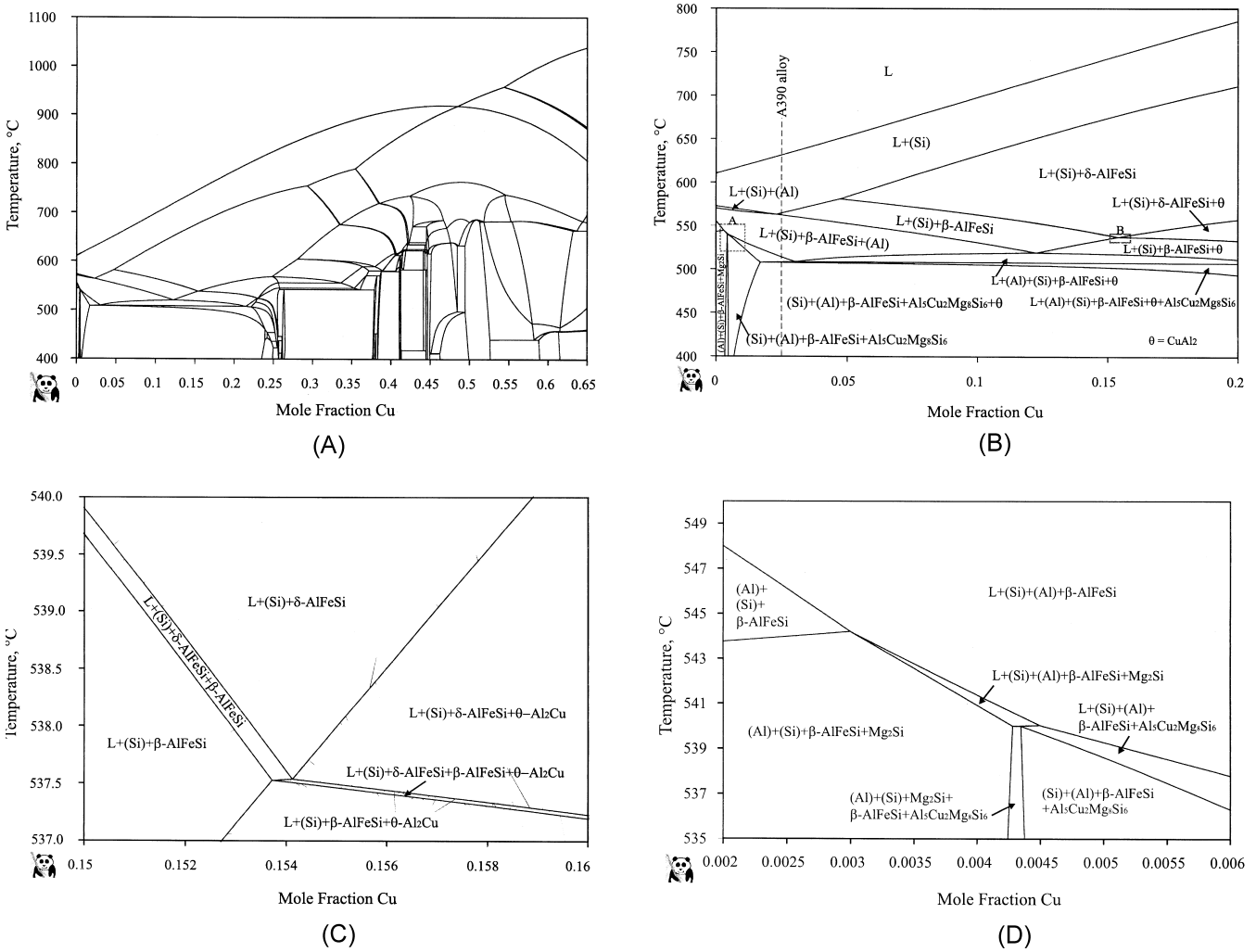

Fig. 11. (A) A calculated isopleth of Al–Cu with fixed values of 0.3% Fe, 0.65% Mg, 0.01% Mn, 15% Si and 0.065% Zn. (B) Al-rich portion of the isopleth given in (A). (C) Enlargement of the region marked 'B' in (B). (D) Enlargement of the region marked 'A' in (B).

equilibrium of L+(Si)+δ-AlFeSi+β-AlFeSi between these two three-phase fields. There is likewise a five-phase field of L+(Si)+δ-AlFeSi+β-AlFeSi+θ, separating the two four-phase fields of L+(Si)+δ-AlFeSi+θ and L+(Si)+β-AlFeSi+θ. Please take note of the temperature and composition coordinates in Fig. 11C; they increase from 537 to 540°C with a change of only 3°C and from 15 mol.% to 16 mol.% Cu with a change of only 1 mol.% Cu. An enlarged region marked 'A' is also displayed in Fig. 11D. These results demonstrate the versatility of the software PANDAT in phase diagram calculations and representations.

Although the traditional liquidus projections have been used effectively in analyzing the paths of solidification for ternary and even for special cases of quaternary alloys, their value is rather limited for higher order alloys even though software programs can be used to calculate this type of diagram. However, software programs can be used to calculate other forms of diagrams for practical utility. For example, we show in Fig. 12 such a diagram giving the calculated phase fractions formed as a function of temperature for alloy 390 under equilibrium conditions. As shown in this figure, the fraction of (Al)+(Si) is more than 94 vol.%, while that of $Al_5Cu_2Mg_8Si_6$ is less than 1.5 vol.%. The fraction of Al_5FeSi(β-AlFeSi) is even less being only 0.15 vol.%. The small amount of the β-AlFeSi phase makes it difficult to detect experimentally in the cast alloys unless extreme care is taken. This will be shown later to be the case. In addition, the temperatures of solidification under the Scheil condition for the formation of primary (Si) and subsequent phases are also given in Table 3 which compared favorably with the experimental data [17].

We will now discuss the freezing ranges and the solidified microstructures of the three alloys AA5182, 7075 and A390 given in Tables 4 and 5. It is evident from

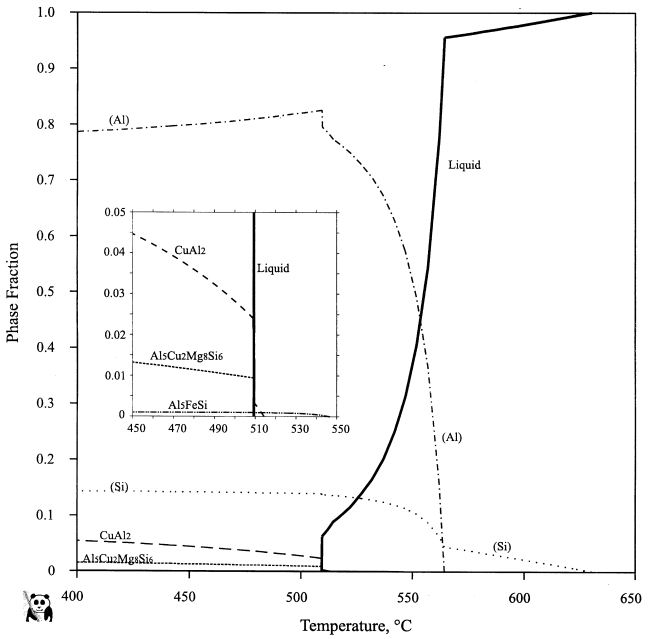

Fig. 12. A calculated phase fraction for alloy A390 showing the fractions of the phases present as a function of temperature under equilibrium condition; the insert shows an enlarged view for the temperature interval from 450 to 550°C.

the data in Table 4 that the measured freezing ranges for AA5182, 7075 and A390 [17] fall in-between those obtained under equilibrium and Scheil conditions as anticipated. Also given in this table are the heats of evolution for these alloys calculated under the Scheil condition. The enthalpy of solidification of pure Al, −10.8 kJ/mol [9] is given for comparison.

As listed in Table 5, the phases in these three solidified alloys calculated under the Scheil condition are in reasonable accord with the experimental data. For AA5182, the phases formed in the solidified alloys as calculated under the Scheil condition and obtained experimentally are identical. For alloy 390, the experimental result does not show the presence of Al_5FeSi (β-AlFeSi) while the calculated result does. This apparent discrepancy can be reconciled when we realize that the fraction of this phase in the solidified alloy is rather small being less than 0.15 vol.% as noted earlier with results presented in Fig. 12.

For the alloy 7075, the three phases (Al), $Al_{13}Fe_3$ and Mg_2Si, were found in the experimental measurements as well as in the calculated results under the Scheil condition.

Table 4
Comparison of ΔT values (the freezing ranges) calculated under equilibrium and Scheil conditions with experimental data as well as the heats or enthalpies of freezing of three aluminum alloys

	5182	7075	390
$\Delta T_{Equi,°C}$	58	131	121
$\Delta T_{Scheil,°C}$	183	169	200
$\Delta T_{Exp't,°C}$	162	161	141
$\Delta H^{Freezing}_{Alloy}$, kJ[a]	−16.3	−16.0	−21.1
$\Delta H^{Freezing}_{Al}$, kJ[a]	−10.8	−10.8	−10.8

[a] kJ/mol of atoms.

In addition, the experimental results also show the presence of fine eutectics and its amount is less than 5 vol.%. Experimental identification of the phases in these eutectics was not without ambiguity and the calculated result containing the phases σ-$(Al,Cu,Zn)_2Mg$ and S-Al_2MgCu might still be correct. We believe solidification of this alloy under controlled experimental conditions such as directional solidification followed by microscopic identification will resolve this minor discrepancy.

3. Conclusion

The results presented in the present paper demonstrate that key experimentally determined phase equilibrium and thermodynamic data are still essential for obtaining phase diagrams of multicomponent systems. However, significant advances have been made since the publication of Alan Prince's book in the use of a computational/experimental approach to generate important phase diagrams of multicomponent systems not only for technological applications but also for fundamental investigation in related fields for materials research. Undoubtedly continual advancement will be made in decades ahead!

Acknowledgements

We wish to thank the Wisconsin Distinguished Professorship, the University-Industry Relations through an I&ER grant and the Department of the Air Force, Wright-Patterson Air Force Base, OH through an SBIR Contract No. F33615-97-C-5276 for financial support.

Table 3
Comparison of calculated reaction temperatures in °C for phases formed in alloy 390 with experimental data

	Primary Si	β-AlFeSi	(Al)	$Al_5Cu_2Mg_8Si_6$	Al_2Cu
Calculated	631	564	562	514	507
Suggested [17]	636	575	561	512	512

Table 5
Metallurgical state of the alloys after solidification

	5182	7075	390
Equilibrium solidified microstructure	(Al)+$Al_{13}Fe_4$ +Mg_2Si	(Al)+$Al_{13}Fe_4$+Mg_2Si	Si+(Al)+Al_5FeSi(β-AlFeSi)+ $Al_5Cu_2Mg_8Si_6$
Scheil solidified microstructure	(Al)+$Al_{13}Fe_4$+Mg_2Si+Al_4Mn +β-Al_8Mg_5	(Al)+$Al_{13}Fe_4$ +Mg_2Si + σ-(Al,Cu,Zn)$_2$Mg+S-Al_2MgCu	Si+(Al)+Al_5FeSi(β-AlFeSi)+ $Al_5Cu_2Mg_8Si_6$+θ-$CuAl_2$
Experimentally solidified microstructure	(Al)+$Al_{13}Fe_4$+Mg_2Si+Al_4Mn +β-Al_8Mg_5	(Al)+$Al_{13}Fe_4$+Mg_2Si +(fine eutectic)	Si+(Al)+$Al_5Cu_2Mg_8Si_6$ +θ-$CuAl_2$

References

[1] K. Matsuyama, Kinzoku-no Kenkyu 11 (10) (1934) 461–490.
[2] D.A. Petrov, N.D. Nagorskaya, Zhurnal Obshchei Khimii 19 (1949) 1994–2037.
[3] G. Phragmen, J. Inst. Metal 77 (1950) 489–552.
[4] D.P. Smith, Metallurgia (1961) 223–231.
[5] H.W.L. Phillips, Aluminium Dev. Assoc., Lond., Inf. Bull. (25) 1961.
[6] A. Prince, Alloy Phase Equilibria, Elsevier, Amsterdam, 1966.
[7] L. Kaufman, H. Bernstein, Computer Calculation of Phase Diagrams, Academic Press, New York, 1970.
[8] T. Chart, High Temp.-High Pressure 5 (1973) 241.
[9] R. Hultgren, P.D. Desai, D.T. Hawkins, M. Glesier, K.K. Kelley, D.D. Wagman, Selected Values of the Thermodynamic Properties of the Elements, American Society for Metals, Metals, Park, OH 44073, 1973.
[10] L.F. Modolfo, Aluminium Alloys: Structure and Properties, 1976.
[11] O. Kubaschewski, in: 5th Edition, Metallurgical Thermochemistry, Pergamon Press, Oxford, 1979.
[12] J. Murray, Int. Metals Rev. 30 (1985) 211.
[13] L. Backerud et al., in: Wrought Alloys, Solidification Characteristics of Aluminum Alloys, Vol. 1, Skanaluminium, 1986.
[14] J. Lacaze, G. Lesoult, O. Relave, I. Ansara, J.P. Riquet, Z. Metallk. 78 (2) (1987) 141–150.
[15] J.L. Murray, Private communication, Alcoa laboratory, Aluminum Co. of America, Alcoa, PA, 1988.
[16] K.-C. Chou, Y.A. Chang, Ber. Bunsenges. Phys. Chem. 93 (1989) 735.
[17] L. Backerud et al., in: Foundry Alloys, Solidification Characteristics of Aluminum Alloys, Vol. 2, AFS/Skanaluminium, 1990.
[18] N. Saunders, Private communication, University of Surrey, UK, 1993.
[19] Y. Zuo, Y.A. Chang, CALPHAD 17 (1993) 177.
[20] N. Saunders, in: Cost 507 Report: Thermochemical Database for Light Metal Alloys, 1994, pp. 19–23, December.
[21] D.J. Chakrabarti, J.L. Murray, Mater. Sci. Forum (1996) 217–222.
[22] S.-L. Chen, Y. Zuo, H. Liang, Y.A. Chang, Metall. Mater. Trans. 28A (1997) 435–446.
[23] H. Liang, Thermodynamic Modeling and Experimental Investigation of the Al–Cu–Mg–Zn Quaternary System, Ph.D. Thesis, University of Wisconsin, Madison, WI, 53706, USA, 1998.
[24] F.-Y. Xie, T. Kraft, Y. Zuo, C.-H. Moon, Y.A. Chang, Acta Mater. 47 (1999) 489–500.
[25] H. Liang, T. Kraft, Y.A. Chang, Mater. Sci. Eng. A 292 (2000) 96–103.
[26] X.-Y. Yan, F.-Y. Xie, M. Chu, Y.A. Chang, Mater. Sci. Eng. A, submitted.
[27] X.-Y. Yan, University of Wisconsin, Madison, WI, 2000, unpublished results.
[28] PANDAT 1.0-Phase Diagram Calculation Engine for Multicomponent Systems, CompuTherm LLC, 437 S. Yellowstone Dr., Suite 217, Madison, Wisconsin, USA, 2000.
[29] F. Zhang, CompuTherm, LLC, 437 S. Yellowstone Dr., Suite 217, Madison, WI 53719, USA, 2000.
[30] E.H. Dix, H.H. Richardson, Trans. AIME 73 (1926) 560.
[31] D. Stockdale, J. Inst. Met. 52 (1933) 111.
[32] H. Auer, Z. Metallkd. 28 (1936) 164.
[33] M.M. Burden, J.D. Hunt, J. Cryst. Growth 22 (1974) 99.